Multi-scale finite element framework for pseudo-2D model

Mingzhao Zhuo[a]

[a]*Faculty of Civil Engineering and Geosciences, Delft University of Technology, Delft, the Netherlands*

Abstract

This manual explain how we use finite element method (FEM) at macro- and micro-scale of a battery cell to solve the pseudo-2D model proposed by Newman and his coworkers.

1. Introduction

Pseudo-2D model was originally proposed by Newman and his coworkers [1, 2] and has been widely applied and developed by following researchers. To solve P2D model, the governing differential equations are usually converted into differential algebraic equations and then solved numerically. However, literatures are quite rare about finite element method [3, 4] for this model. Here we propose FEM at both scales and connect the two-scale computations by downscaling pore wall flux and upscaling surface lithium concentration and its derivative with respect to the downscaled flux. The derivative term is needed for faster convergence, but it was not passed back in COMSOL 3.5a as Fig. 2 shows in Ref. [5].

2. Govenring equations of P2D model

2.1. Microscale diffusion in active material particles

In the solid particle, we consider the diffusion process of lithium. The conservation of lithium species inside the particle can be written as

$$\frac{\partial c_s}{\partial t} + \frac{1}{r^2}\frac{\partial}{\partial r}\left[r^2\left(-D_s\frac{\partial c_s}{\partial r}\right)\right] = 0, \tag{1}$$

where c_s and D_s (c_s) denote the lithium concentration and the bulk solid-state diffusion coefficient of lithium, respectively, inside the active material phase. Here the bulk coefficient could be constant or concentration c_s dependent. The FEM simulation at microscale does not necessarily require linear diffusion, as analytical approach does.

2.2. Macroscale conservation equations at cell level

The cell consists of anode, separator, and cathode (Fig. 1). At the cell level, the anode and cathode have solid phase (electronic conduction ϕ_s) and electrolyte phase (ionic conduction ϕ_e and lithium ion transport c_e). The separator only has the electrolyte phase.

Email addresses: m.zhuo@tudelft.nl (Mingzhao Zhuo), mzzhuo@gmail.com (Mingzhao Zhuo)

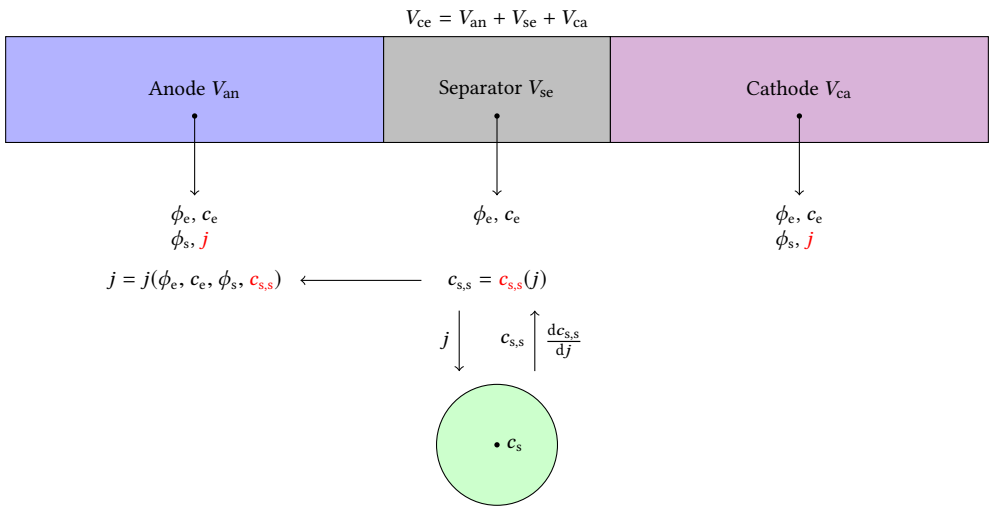

Fig. 1. Schematic of the battery cell. Micro problem is 3D, and macro problem can be 1D, 2D, and 3D.

Conservation of electric charge in the solid phase of two electrodes implies that

$$\nabla \cdot \left(-\sigma^{\text{eff}} \nabla \phi_s\right) = -aFj, \tag{2}$$

where σ^{eff} and ϕ_s denote the effective electronic conductivity and electric potential inside the electrode phase, respectively. Here a denotes the active particle surface area per unit electrode volume:

$$a = \frac{4\pi R_s^2}{4/3\pi R_s^3}\epsilon_s = \frac{3\epsilon_s}{R_s}. \tag{3}$$

F is Faraday's constant, and j is the pore wall flux from the active particle to the electrolyte (*i.e.,* positive j means mass flux from particle to electrolyte and vice versa).

Conservation of lithium ion in the electrolyte phase of the whole cell (two electrodes and separator) can be expressed as

$$\epsilon_e \frac{\partial c_e}{\partial t} + \nabla \cdot \left(-D_e^{\text{eff}} \nabla c_e\right) = (1 - t_e)aj, \tag{4}$$

where c_e denotes the lithium-ion concentration, D_e^{eff} is the effective diffusion coefficient, t_e is the lithium-ion transference number.

Conservation of electric charge in the electrolyte phase of the whole cell is written as

$$\nabla \cdot \left(-\kappa^{\text{eff}} \nabla \phi_e + \kappa_D^{\text{eff}} \nabla \ln c_e\right) = aFj, \tag{5}$$

where κ^{eff} is the effective ionic conductivity and ϕ_e is the electric potential. κ_D^{eff} is expressed as

$$\kappa_D^{\text{eff}} = \frac{2RT\kappa^{\text{eff}}}{F}\left(1 + \frac{\partial \ln f_e}{\partial \ln c_e}\right)(1 - t_e), \tag{6}$$

where T is the temperature and f_e is the mean activity coefficient.

The effective electronic conductivity σ^{eff}, effective electrolyte diffusivity D_e^{eff}, and ionic conductivity κ^{eff} are given by Bruggemen's relation:

$$\sigma^{\text{eff}} = \sigma\epsilon_s^{\alpha}, \quad D_e^{\text{eff}} = D_e\epsilon_e^{\alpha}, \quad \kappa^{\text{eff}} = \kappa\epsilon_e^{\alpha},$$

where $\alpha = 1.5$. $\sigma\ (c_s)$, $D_e\ (c_e)$, and $\kappa\ (c_e)$ are the bulk material properties and they can be concentration dependent.

Remarks: material property σ may take different values in the anode and cathode. ϵ_s and ϵ_e also may take different values in anode, cathode, and separator. Volumetric surface area $a\ (\mathbf{x})$ can take different values at any point of anode and cathode.

2.3. Bulter-Volmer equation

We assume the pore wall flux at the active material-electrolyte interface to be governed by the widely used Butler-Volmer equation:

$$j = \frac{i_0}{F}\left[\exp\left(\frac{\alpha_a F}{RT}\eta\right) - \exp\left(-\frac{\alpha_c F}{RT}\eta\right)\right] = j_0\,\text{BV}(\eta), \tag{7}$$

where $i_0 = j_0 F$ is the exchange current density, α_a and α_c are the anodic and cathodic transfer coefficients, and η is the interfacial overpotential. The exchange current density i_0 is written as

$$i_0 = kFc_{s,s}^{\alpha_c}(c_{s,\max} - c_{s,s})^{\alpha_a}c_e^{\alpha_a}, \tag{8}$$

where $k\ \left(\text{m}^{2.5}\text{mol}^{-0.5}\text{s}^{-1}\right)$ is the rate constant of the charge transfer reaction, $c_{s,\max}$ is the maximum saturation concentration of intercalated lithium, and $c_{s,s}$ is the surface lithium concentration. The overpotential η is expressed as

$$\eta = \phi_s - \phi_e - U_{\text{oc}}, \tag{9}$$

where the equilibrium potential U_{oc} can be modeled as function of the surface concentration $c_{s,s}$ in active material.

Remarks: $\phi_s\ (\mathbf{x})$, $\phi_e\ (\mathbf{x})$, and $c_e\ (\mathbf{x})$ are variables defined at the macroscale, while $c_{s,s}\ (\mathbf{x})$ is value of microscale variable $c_s(\mathbf{x}, r)$ at particle surface $r = R_s$.

3. Coupled finite element framework

This section outlines the procedures to solve the governing equations within multi-scale FEM framework. The equations to solve are Eq. (1) at microscale for $c_s\ (\mathbf{x}, r, t)$ and Eqs. (2), (4) and (5) at macroscale for $\phi_s(\mathbf{x}, t)$, $\phi_e(\mathbf{x}, t)$,

$c_e(\mathbf{x}, t)$.

Apparently, the computational domain for the two scales are different. At the macroscale, Eqs. (2), (4) and (5) are defined on three computational regions—anode, separator, and cathode: Eq. (2) is defined on anode and cathode, and Eqs. (4) and (5) are defined on the whole battery cell, two electrodes plus the separator. At different regions, material properties and porosity can be different. At the microscale, the computational domain is a single active particle attached to each node of the macroscopic mesh.

To apply FEM at both scales simultaneously, we need to establish the connection between the FEM simulations at two scales. For all of these Eqs. (2), (4) and (5), the source terms involving an extra unknown j, the pore wall flux. To this end, we assign a 4th and a 3rd degree of freedom to any node in electrode domain and any node in the separator domain, respectively. An interface node between electrode and separator has 4 dofs, same as those inside electrodes. Accordingly, we need to add one more equation for this extra dof, that is, the Bulter-Volmer equation (7). We note that the pore wall flux is a function of not only the three macroscale field variables, but also a macroscale quantity $c_{s,s}$ derived from microscale solution:

$$j(\mathbf{x}, t) = j(\phi_s, \phi_e, c_e, c_{s,s}). \tag{10}$$

Eq. (10) implies that macroscale solution depends on the microscale information $c_{s,s}$. From the perspective of microscale computation, it simply needs the pore wall flux j, which comes from macroscale simulation, as the Neumann boundary condition.

Thus the microscale FEM computation can serve as the relation between $c_{s,s}$ and j: $c_{s,s} = c_{s,s}(j)$. With this substituted into Eq. (10), we can complete the equations at macroscale. In addition to $c_{s,s}$, we also need to upscale its derivative with respect to j, $\frac{\mathrm{d}c_{s,s}}{\mathrm{d}j}$, for faster convergence.

4. FEM implementation

This section provides FEM implementation of solving the governing equations. To this end, the index notation is used for vector and matrix operations. If not familiar with index notation, readers are referred to textbooks [6] for more details.

4.1. Diffusion in active particles

To consider particles of different radius, we scale the length r by particle radius R_s. We also define a reference diffusivity D_s^{ref} to scale the diffusivity, which can be concentration dependent, in the solids.

$$x = \frac{r}{R_s}, \quad D_s^* = \frac{D_s}{D_s^{\mathrm{ref}}}. \tag{11}$$

We then partially nondimensionalize Eq. (1) and get

$$\frac{R_s^2}{D_s^{\mathrm{ref}}} \frac{\partial c_s}{\partial t} + \frac{1}{x^2} \frac{\partial}{\partial x} \left[x^2 \left(-D_s^* \frac{\partial c_s}{\partial x} \right) \right] = 0. \tag{12}$$

Now we write the weak form of this equation, the integal form over scaled domain, sphere of unit radius:

$$\frac{R_s^2}{D_s^{\text{ref}}}\int_0^1 \frac{\partial c_s}{\partial t} 4\pi x^2 \hat{c}_s \,\mathrm{d}x + \int_0^1 \frac{\partial}{\partial x}\left[x^2\left(-D_s^* \frac{\partial c_s}{\partial x}\right)\right] 4\pi \hat{c}_s \,\mathrm{d}x = 0, \tag{13}$$

where $\hat{c}_s$ is the variation of field variable c_s. Applying Gauss's theorem to the second term, we obtain

$$\frac{R_s^2}{D_s^{\text{ref}}}\int_0^1 \frac{\partial c_s}{\partial t} 4\pi x^2 \hat{c}_s \,\mathrm{d}x + \int_0^1 4\pi x^2 D_s^* \frac{\partial c_s}{\partial x}\frac{\partial \hat{c}_s}{\partial x}\,\mathrm{d}x + 4\pi x^2\left(-D_s^* \frac{\partial c_s}{\partial x}\right)\hat{c}_s\Big|_0^1 = 0. \tag{14}$$

At the external node $x = 1$,

$$Q = 4\pi \left(-D_s^* \frac{\partial c_s}{\partial x}\right)\Big|_1 = -\frac{4\pi R_s}{D_s^{\text{ref}}}\, D_s \frac{\partial c_s}{\partial r}\Big|_1 = -\frac{4\pi R_s}{D_s^{\text{ref}}} j. \tag{15}$$

Next we discretize the domain and express the continuous variable c_s using the nodal unknowns:

$$c_s = N^i c_s^i, \quad \hat{c}_s = N^j \hat{c}_s^j. \tag{16}$$

Substituting Eq. (16) into Eq. (14) and considering it holds for each $\hat{c}_s^j$, we thus get

$$f^j = \frac{R_s^2}{D_s^{\text{ref}}}\int_0^1 \frac{c_{s,n}^i - c_{s,n-1}^i}{\Delta t} 4\pi x^2 N^i N^j \,\mathrm{d}x + \int_0^1 4\pi x^2 D_s^* \frac{\partial N^i}{\partial x}\frac{\partial N^j}{\partial x} c_s^i \,\mathrm{d}x + 4\pi x^2\left(-D_s^* \frac{\partial c_s}{\partial x}\right)N_j\Big|_0^1 = 0. \tag{17}$$

Note that here we use implicit time scheme and thus c_s^i represents $c_{s,n}^i$ at time step n. Newton-Raphson iteration method is used to solve Eq. (17), and the stiffness matrix is expressed as

$$K_{ji} = \frac{\partial f^j}{\partial c_s^i} = \frac{R_s^2}{D_s^{\text{ref}}}\int_0^1 \frac{4\pi x^2 N^i N^j}{\Delta t}\,\mathrm{d}x + \int_0^1 4\pi x^2 D_s^* \frac{\partial N^i}{\partial x}\frac{\partial N^j}{\partial x}\,\mathrm{d}x \tag{18}$$

Remarks: The implementation is in one-dimensional domain but results are for three-dimension.

4.2. Cell level

Next we write the weak forms of Eqs. (2), (4) and (5) and obtain

$$\int_{V_{\text{ce}}} \boldsymbol{\nabla}\cdot\left(-\kappa^{\text{eff}}\boldsymbol{\nabla}\phi_e + \kappa_D^{\text{eff}}\boldsymbol{\nabla}\ln c_e\right)\hat{\phi}_e \,\mathrm{d}V - \int_{V_{\text{ce}}} aFj\,\hat{\phi}_e \,\mathrm{d}V = 0, \tag{19}$$

$$\int_{V_{\text{ce}}} \frac{\partial c_e}{\partial t}\hat{c}_e \,\mathrm{d}V + \int_{V_{\text{ce}}} \boldsymbol{\nabla}\cdot\left(-D_e^{\text{eff}}\boldsymbol{\nabla}c_e\right)\hat{c}_e \,\mathrm{d}V - \int_{V_{\text{ce}}} (1-t_e)aj\,\hat{c}_e \,\mathrm{d}V = 0, \tag{20}$$

$$\int_{V_{\text{an}}+V_{\text{ca}}} \boldsymbol{\nabla}\cdot\left(-\sigma^{\text{eff}}\boldsymbol{\nabla}\phi_s\right)\hat{\phi}_s \,\mathrm{d}V + \int_{V_{\text{an}}+V_{\text{ca}}} aFj\,\hat{\phi}_s \,\mathrm{d}V = 0. \tag{21}$$

Applying Gauss's theorem, we obtain

$$\int_{V_{\mathrm{ce}}} \kappa^{\mathrm{eff}} \boldsymbol{\nabla}\phi_{\mathrm{e}} \cdot \boldsymbol{\nabla}\hat{\phi}_{\mathrm{e}} \,\mathrm{d}V - \int_{V_{\mathrm{ce}}} \kappa_{\mathrm{D}}^{\mathrm{eff}} \boldsymbol{\nabla} \ln c_{\mathrm{e}} \cdot \boldsymbol{\nabla}\hat{\phi}_{\mathrm{e}} \,\mathrm{d}V + \int_{\partial V_{\mathrm{ce}}} \mathbf{i}_{\mathrm{e}} \cdot \mathbf{n}\, \hat{\phi}_{\mathrm{e}} \,\mathrm{d}A - \int_{V_{\mathrm{ce}}} aFj\, \hat{\phi}_{\mathrm{e}} \,\mathrm{d}V = 0, \tag{22}$$

$$\int_{V_{\mathrm{ce}}} \frac{\partial c_{\mathrm{e}}}{\partial t}\, \hat{c}_{\mathrm{e}} \,\mathrm{d}V + \int_{V_{\mathrm{ce}}} D_{\mathrm{e}}^{\mathrm{eff}} \boldsymbol{\nabla} c_{\mathrm{e}} \cdot \boldsymbol{\nabla}\hat{c}_{\mathrm{e}} \,\mathrm{d}V + \int_{\partial V_{\mathrm{ce}}} \mathbf{q}_{\mathrm{e}} \cdot \mathbf{n}\, \hat{c}_{\mathrm{e}} \,\mathrm{d}A - \int_{V_{\mathrm{ce}}} (1 - t_{\mathrm{e}}) aj\, \hat{c}_{\mathrm{e}} \,\mathrm{d}V = 0, \tag{23}$$

$$\int_{V_{\mathrm{an}}+V_{\mathrm{ca}}} \sigma^{\mathrm{eff}} \boldsymbol{\nabla}\phi_{\mathrm{s}} \cdot \boldsymbol{\nabla}\hat{\phi}_{\mathrm{s}} \,\mathrm{d}V + \int_{\partial V_{\mathrm{an}}+\partial V_{\mathrm{ca}}} \mathbf{i}_{\mathrm{s}} \cdot \mathbf{n}\, \hat{\phi}_{\mathrm{s}} \,\mathrm{d}V + \int_{V_{\mathrm{an}}+V_{\mathrm{ca}}} aFj\, \hat{\phi}_{\mathrm{s}} \,\mathrm{d}V = 0. \tag{24}$$

Expressing variables as interpolation of their nodal values:

$$\phi_{\mathrm{e}} = N^i \phi_{\mathrm{e}}^i, \quad c_{\mathrm{e}} = N^i c_{\mathrm{e}}^i, \quad \phi_{\mathrm{s}} = N^i \phi_{\mathrm{s}}^i, \quad j = N^i j^i, \tag{25}$$

$$\hat{\phi}_{\mathrm{e}} = N^j \hat{\phi}_{\mathrm{e}}^j, \quad \hat{c}_{\mathrm{e}} = N^j \hat{c}_{\mathrm{e}}^j, \quad \hat{\phi}_{\mathrm{s}} = N^j \hat{\phi}_{\mathrm{s}}^j. \tag{26}$$

Discretizing Eqs. (2), (4) and (5) and Bulter-Volmer equation gives

$$f_{\phi}^j = \int_{V_{\mathrm{ce}}} \kappa^{\mathrm{eff}} \frac{\partial N^i}{\partial x_k} \frac{\partial N^j}{\partial x_k} \phi_{\mathrm{e}}^i \,\mathrm{d}V - \int_{V_{\mathrm{ce}}} \kappa_{\mathrm{D}}^{\mathrm{eff}} \frac{1}{N^m c_{\mathrm{e}}^m} \frac{\partial N^i}{\partial x_k} \frac{\partial N^j}{\partial x_k} c_{\mathrm{e}}^i + \int_{\partial V_{\mathrm{ce}}} \mathbf{i}_{\mathrm{e}} \cdot \mathbf{n}\, N^j \,\mathrm{d}A - \int_{V_{\mathrm{ce}}} aFN^i j^i\, N^j \,\mathrm{d}V \qquad = 0, \tag{27a}$$

$$f_{\mathrm{c}}^j = \int_{V_{\mathrm{ce}}} \frac{c_{\mathrm{s},n}^i - c_{\mathrm{s},n-1}^i}{\Delta t} N^i N^j \,\mathrm{d}V + \int_{V_{\mathrm{ce}}} D_{\mathrm{e}}^{\mathrm{eff}} \frac{\partial N^i}{\partial x_k} \frac{\partial N^j}{\partial x_k} c_{\mathrm{e}}^i \,\mathrm{d}V + \int_{\partial V_{\mathrm{ce}}} \mathbf{q}_{\mathrm{e}} \cdot \mathbf{n}\, N^j \,\mathrm{d}A - \int_{V_{\mathrm{ce}}} (1 - t_{\mathrm{e}}) aN^i j^i\, N^j \,\mathrm{d}V = 0, \tag{27b}$$

$$f_{\mathrm{s}}^j = \int_{V_{\mathrm{an}}+V_{\mathrm{ca}}} \sigma^{\mathrm{eff}} \frac{\partial N^i}{\partial x_k} \frac{\partial N^j}{\partial x_k} \phi_{\mathrm{s}}^i \,\mathrm{d}V + \int_{\partial V_{\mathrm{an}}+\partial V_{\mathrm{ca}}} \mathbf{i}_{\mathrm{s}} \cdot \mathbf{n}\, N^j \,\mathrm{d}V + \int_{V_{\mathrm{an}}+V_{\mathrm{ca}}} aFN^i j^i\, N^j \,\mathrm{d}V \qquad = 0, \tag{27c}$$

$$f_{\mathrm{q}}^i = j^i - j_0\left(c_{\mathrm{s,s}}^i, c_{\mathrm{e}}^i\right) \mathrm{BV}\left(\phi_{\mathrm{s}}^i - \phi_{\mathrm{e}}^i - U_{\mathrm{oc}}\left(c_{\mathrm{s,s}}^i\right)\right) \qquad = 0. \tag{27d}$$

To use Newton-Raphson iteration, we write the stiffness matrix as

$$K_{ji}^{\phi\phi} = \frac{\partial f_{\phi}^{j}}{\partial \phi_{e}^{i}} = \int_{V_{ce}} \kappa^{\text{eff}} \frac{\partial N^{i}}{\partial x_{k}} \frac{\partial N^{j}}{\partial x_{k}} \, \mathrm{d}V \tag{28a}$$

$$K_{ji}^{\phi c} = \frac{\partial f_{\phi}^{j}}{\partial c_{e}^{i}} = -\int_{V_{ce}} \kappa_{D}^{\text{eff}} \frac{1}{N^{m} c_{e}^{m}} \frac{\partial N^{i}}{\partial x_{k}} \frac{\partial N^{j}}{\partial x_{k}} \, \mathrm{d}V + \int_{V_{ce}} \kappa_{D}^{\text{eff}} \frac{N^{i}}{\left(N^{m} c_{e}^{m}\right)^{2}} \frac{\partial N^{n}}{\partial x_{k}} \frac{\partial N^{j}}{\partial x_{k}} c_{e}^{n} \, \mathrm{d}V \tag{28b}$$

$$K_{ji}^{\phi q} = \frac{\partial f_{\phi}^{j}}{\partial j^{i}} = -\int_{V_{ce}} aF \, N^{i} \, N^{j} \, \mathrm{d}V \tag{28c}$$

$$K_{ji}^{cc} = \frac{\partial f_{c}^{j}}{\partial c_{e}^{i}} = \int_{V_{ce}} \frac{1}{\Delta t} \, N^{i} N^{j} \, \mathrm{d}V + \int_{V_{ce}} D_{e}^{\text{eff}} \frac{\partial N^{i}}{\partial x_{k}} \frac{\partial N^{j}}{\partial x_{k}} \, \mathrm{d}V \tag{28d}$$

$$K_{ji}^{cq} = \frac{\partial f_{c}^{j}}{\partial j^{i}} = -\int_{V_{ce}} (1 - t_{e}) a \, N^{i} \, N^{j} \, \mathrm{d}V \tag{28e}$$

$$K_{ji}^{ss} = \frac{\partial f_{s}^{j}}{\partial \phi_{s}^{i}} = \int_{V_{an}+V_{ca}} \sigma^{\text{eff}} \frac{\partial N^{i}}{\partial x_{k}} \frac{\partial N^{j}}{\partial x_{k}} \, \mathrm{d}V \tag{28f}$$

$$K_{ji}^{sq} = \frac{\partial f_{s}^{j}}{\partial j^{i}} = \int_{V_{an}+V_{ca}} aF \, N^{i} \, N^{j} \, \mathrm{d}V \tag{28g}$$

$$K_{ji}^{qq} = \frac{\partial f_{q}^{j}}{\partial j^{i}} = \delta_{ij} - \left(\frac{\partial j_{0}}{\partial c_{s,s}^{i}} \mathrm{BV}\left(\phi_{s}^{i} - \phi_{e}^{i} - U_{oc}\right) - j_{0} \frac{\partial \mathrm{BV}}{\partial U_{oc}} \frac{\partial U_{oc}}{\partial c_{s,s}^{i}} \right) \frac{\partial c_{s,s}^{i}}{\partial j^{i}} \delta_{ij} \tag{28h}$$

$$K_{ji}^{q\phi} = \frac{\partial f_{q}^{j}}{\partial \phi_{e}^{i}} = -j_{0} \frac{\partial \mathrm{BV}}{\partial \phi_{e}^{i}} \delta_{ij} \tag{28i}$$

$$K_{ji}^{qc} = \frac{\partial f_{q}^{j}}{\partial c_{e}^{i}} = -\frac{\partial j_{0}}{\partial c_{e}^{i}} \delta_{ij} \mathrm{BV}\left(\phi_{s}^{i} - \phi_{e}^{i} - U_{oc}\right) \tag{28j}$$

$$K_{ji}^{qs} = \frac{\partial f_{q}^{j}}{\partial \phi_{s}^{i}} = -j_{0} \frac{\partial \mathrm{BV}}{\partial \phi_{s}^{i}} \delta_{ij} \tag{28k}$$

Note that in Eqs. (27d) and (28h), the nodal surface concentration $c_{s,s}^{i}$ and its derivative with respect to the nodal pore wall flux j^{i} are obtained from microscale simulation. If the derivative term is not upscaled, the convergence rate is way slower.

5. Verification

Here we compare our results with COMSOL simulation results performed by Han et. al. [7]. All simulation parameters can be found in Ref. [7].

References

[1] M. Doyle, T. F. Fuller, J. Newman, Modeling of Galvanostatic Charge and Discharge of the Lithium/Polymer/Insertion Cell, Journal of The Electrochemical Society 140 (6) (1993) 1526. doi:10.1149/1.2221597.

[2] M. Doyle, J. Newman, A. S. Gozdz, C. N. Schmutz, J. Tarascon, Comparison of Modeling Predictions with Ex-

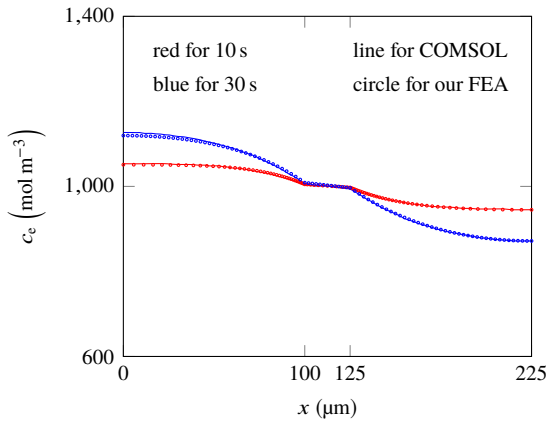

Fig. 2. Electrolyte concentration distribution at 1C discharge. COMSOL results are reported in Ref. [7].

perimental Data from Plastic Lithium Ion Cells, Journal of The Electrochemical Society 143 (6) (1996) 1890. doi:10.1149/1.1836921.

[3] S. Golmon, K. Maute, M. L. Dunn, Numerical modeling of electrochemical–mechanical interactions in lithium polymer batteries, Computers & Structures 87 (23-24) (2009) 1567–1579. doi:10.1016/j.compstruc.2009.08.005.

[4] M. Guo, X. Jin, R. E. White, Nonlinear state-variable method (NSVM) for li-ion batteries: Finite-element method and control mode, Journal of The Electrochemical Society 164 (11) (2017) E3200–E3214. doi:10.1149/2.0221711jes.

[5] L. Cai, R. E. White, Mathematical modeling of a lithium ion battery with thermal effects in COMSOL inc. multiphysics (MP) software, Journal of Power Sources 196 (14) (2011) 5985–5989. doi:10.1016/j.jpowsour.2011.03.017.

[6] A. F. Bower, Applied Mechanics of Solids, CRC Press, 2009. doi:10.1201/9781439802489.

[7] X. Han, M. Ouyang, L. Lu, J. Li, Simplification of physics-based electrochemical model for lithium ion battery on electric vehicle. part i: Diffusion simplification and single particle model, Journal of Power Sources 278 (2015) 802–813. doi:10.1016/j.jpowsour.2014.12.101.